MnO, Co and Ni Nanoparticle Synthesis by Oleylamie and Oleic Acid

*Wencai He[a], Yifang Qi[a], Uppalaiah Erugu[b], Jaiden Moore[a], Xianchun Zhu[a], Teresa Demeritte[a], Fengxiang Han[a], Jinke Tang[b], Qilin Dai[a]**

[a]Department of Chemistry, Physics, and Atmospheric Sciences, Jackson State University, Jackson, MS, 39217, United States

[b] Department of Physics & Astronomy, University of Wyoming Laramie, Wyoming 82071, USA

[*]Corresponding author Email address: qilin.dai@jsums.edu (QD)

Abstract

Magnetic nanoparticles are attracting much attention toward easy operation and size controlable synthesis methods. We develop a method to synthesize MnO, Co, CoO, and Ni nanoparticles by thermal decomposition of metal 2,4-pentanedionates in the presence of oleylamine (OLA), oleic acid (OA), and 1-octadecene (ODE). Similar experimental conditions are used to prepare nanoparticles except for the metal starting materials (manganese 2,4-pentanedionate, nickel 2,4-pentanedionate, and cobalt 2,4-pentanedionate), leading to different products. For the manganese 2,4-pentanedionate starting material, MnO nanoparticles are always obtained as the reaction is controlled with different temperatures, precursor concentrations, ligand ratios, and reaction time. For the cobalt 2,4-pentanedionate starting material, only three experimental conditions can produce pure phase CoO and Co nanoparticles. For the nickel 2,4-pentanedionate starting material, only three experimental conditions lead to the production of pure phase Ni nanoparticles. The nanoparticle sizes increase with the increase of reaction temperatures. It is observed that the reaction time affects nanoparticle growth. The nanoparticles are studied by XRD, TEM, and magnetic measurements. This work presents a facile method to prepare nanoparticles with different sizes, which provides a fundamental understanding of nanoparticle growth in solution.

Introduction

Magnetic nanoparticles are extensively studied due to their applications in energy storage, biomedical research, hypothermia treatment, solar energy transformers, catalysis, and water purification.[1–7] CoO and MnO nanoparticles have been synthesized by a lot of methods including the solvothermal method, thermolysis method, and solid-state oxidation.[8–10] Co and Ni nanoparticles were synthesized by organometallic compounds [$Co_2(CO)_8$] in some organic solvents and stabilizers.[8,11] Lu *et al.* reported that Co nanoparticles can be produced by the reduction of $CoCl_2$ using $NaBH_4$ in polymers. Laser ablation was reported to prepare Co nanoparticles by the decomposition of $Co_2(CO)_8$.[12] Ni nanoparticles were synthesized by an arc discharge process,[13] microwave method with polyvinyl pyrrolidone and dodecylamine,[14] reduction of $Ni(NO_3)_2$ in polyethylene glycol,[15] reduction of $Ni(acac)_2$ by oleylamine,[16] reduction of $Ni(NO_3)_2 \cdot 6H_2O$ by benzildiethylenetriamine.[17] However, the reported methods are very complicated, or special starting materials are required for the methods.

We reported a facile method to prepare CoO, Co, and MnO nanocrystals by metal acetates in the presence of oleylamine, oleic acid, and ODE under the protection of the nitrogen atmosphere.[18] It is observed that the nanoparticle sizes are ranging from 50 nm to several hundred nanometers.[18] The size distribution is also very broad. This is attributed to the metal source of metal acetates. It is reported that the metal 2,4-pentanedionates can produce smaller nanoparticles controlled by the reaction atmosphere.[18,19] Therefore, it is worth studying the preparation of metal or metal oxide nanoparticles by metal 2,4-pentanedionates in the presence of oleylamine and oleic acid.

In this work, MnO, Co, and Ni nanoparticles are synthesized by metal 2,4-pentanedionates in the presence of oleylamine and oleic acid. The reaction temperatures, reaction time, precursor concentrations, and ligand ratios are used to control the synthesis of the nanoparticles. nanoparticles with sizes of 20-500 nm are obtained. The magnetic properties of MnO and CoO and Co nanoparticles are also studied. MnO nanoparticles show traditional paramagnetic properties. CoO nanoparticles show ferromagnetic behavior due to the uncompensated spins on the surface. Co nanoparticles exhibit traditional ferromagnetic properties. Magnetic concentration cells based on Co and CoO nanoparticles are fabricated and investigated. The Co-based cell shows better performance than that of the CoO-based cell.

Methods and Materials

2.1. Chemicals and materials

Manganese (II) 2,4-pentanedionate ($Mn(acac)_2$, $MnC_5H_7O_2)_2$), Nickel (II) 2,4-pentanedionate ($Ni(acac)_2$, Ni $(C_5H_7O_2)_2$, 95%) and oleic acid (OA, tech, 90%) were purchased from Alfa Aesar. Cobalt (III) 2, 4-pentanedionate ($Co(acac)_3$, Co $(C_5H_7O_2)_3$, 95%) was purchased from Chem-impex Int'l Inc. Oleylamine (OLA, >50%) was purchased from TCI America. 1-octadecene (ODE, tech, 90%) was purchased from Acros Organics. Acetone (CH_3COCH_3, tech) was purchased from Aqua Solutions, Inc. Toluene (99.9%) was purchased from Fisher Chemical. All chemicals were used without further purification.

2.2. Synthesis of nanoparticles

The required amount of manganese (II) 2, 4-pentanedionate, OLA, and OA (see Table 1) were loaded in a 100 ml 3-neck round-bottomed flask, and the flask was degassed 3 times at room temperature. Then, the mixture was heated for 1 hour at 120 °C under vacuum followed by degassing 3 times at 120 °C. Afterward, the solution was heated to designed temperatures and kept

for different hours (see Table 1). Then the heat was removed and the reaction mixture was cooled down to room temperature naturally. The nanoparticles were centrifuged at 3000 rpm for 5 min, then re-dispersed in toluene, finally precipitated with acetone. The powders were obtained by drying at 60 °C under vacuum for XRD measurements. The procedures for the preparation of Ni, Co, and Ni nanoparticles are very similar to MnO synthesis except for the starting materials.

2.3. Measurements

Powder X-ray diffraction (XRD) results were obtained with a MiniFlex 600 Rigaku X-ray Diffractometer. The magnetic hysteresis (M-H) loops of the powders were measured on a Physical Properties Measurement System (PPMS) from Quantum Design at room temperature. A plastic container with two 0.4 mm thick copper sheets was used to measure the magnetic electrolyte concentration cell device performance. The I-T and V-T curves are obtained by Keithley 2400 and CHI 604E, respectively. Magnetic fields provided by a magnet (Master Magnetics) were used to switch directions every 30 s. The morphology of nanocrystals was studied by a transmission electron microscope (TEM) (JEM-1011, JEOL).

Table 1 MnO sample information in this work

Sample	$Mn(acac)_2$/g	OA/mL	OLA/ mL	ODE/ mL	Temperature /°C	Time/h
S1	2	10	10	0	200	2
S2	2	10	10	0	250	2
S3	2	10	10	0	280	2
S4	2	10	10	0	300	2
S5	2	10	10	20	300	2
S6	2	10	10	40	300	2
S7	2	10	0	0	300	2
S8	2	10	1	0	300	2

S9	2	10	5	0	300	2
S10	2	10	20	0	300	2
S11	2	10	30	0	300	2
S12	2	0	10	0	300	2
S13	2	10	10	0	300	1
S14	2	10	10	0	300	4
S15	2	10	10	0	300	6

Table 2 Co and CoO sample information in this work

Sample	$Co(acac)_3$/g	OA/ mL	OLA/ mL	ODE/ mL	Temperature /°C	Time/h
S16	2	10	20	0	300	2
S17	2	10	30	0	300	2
S18	2	0	10	0	300	2

Table 3 Ni sample information in this work

Sample	$Ni(acac)_2$/g	OA/ mL	OLA/ mL	ODE/ mL	Temperature /°C	Time/h
S19	2	10	20	0	300	2
S20	2	10	30	0	300	2
S21	2	0	10	0	300	2

Results and discussion

All the samples S2-S15 in this work are indexed to a pure cubic phase of MnO according to the standard card of JCPDS 07-0230 (Figure S1). Different temperatures including 200 ºC, 250 ºC, 280 ºC, 300 ºC are used to synthesize nanoparticles (S1, S2, S3, and S4). No nanoparticles are obtained for S1 since the reaction temperature is too low for the decomposition of metal 2, 4-pentanedionates. Figures 1 a, b, and c show the TEM images of S2, S3, and S4. It can be seen that the size distribution of S2 prepared at 250 ºC is very broad. The sizes are in the range of 100-200 nm. The average size of S2 is 98 nm. The average sizes increase to 387 nm and 525 nm for the reaction temperatures of 280 ºC and 300 ºC, respectively (figure 1b S3 and c S4). The nanoparticle sizes increase from 98 nm to 525 nm as the reaction temperature increases from 250 ºC to 300 ºC. The increased sizes are explained by the increasing temperatures.[20–22] The Ostwald ripening process is enhanced by the high temperature significantly, leading to increased nanoparticle sizes.

ODE is utilized as a noncoordinating ligand in this reaction to study the influence of precursor concentrations on the size and morphology of MnO nanoparticles. S5 and S6 are prepared with ODE of 20 mL and 40 mL, respectively, with the same experimental condition of S4. Figures 1d and e show the TEM images of S5 and S6. The average sizes of S5 and S6 are 415 nm and 263 nm, respectively. It can be seen that the sizes are 525 nm, 415 nm, and 263 nm as the reaction precursor concentrations decrease (S4, S5, and S6). Therefore, the sizes decrease with the increase of the precursor concentration. The distance between seed crystals increases as the precursor concentration increases, leading to decreased seed crystal aggregation and smaller sizes of the nanoparticles.[23] It is also related to the ligands of oleylamine and oleic acid.[23] It is reported that the ratios of OLA to OA can play a role in capping the nanoparticles, leading to different morphology and sizes.[24–26] The amount of OLA ranging from 0 to 30 mL is employed to

investigate the influence of OLA on the size and morphology of the MnO nanoparticles. S7 does not exhibit any nanoparticles as the only OA is used in the reaction (without OLA). Figure 1f-j shows the TEM images of S8-S12. The OLA amount increases from 0 to 30 mL as the OA amount

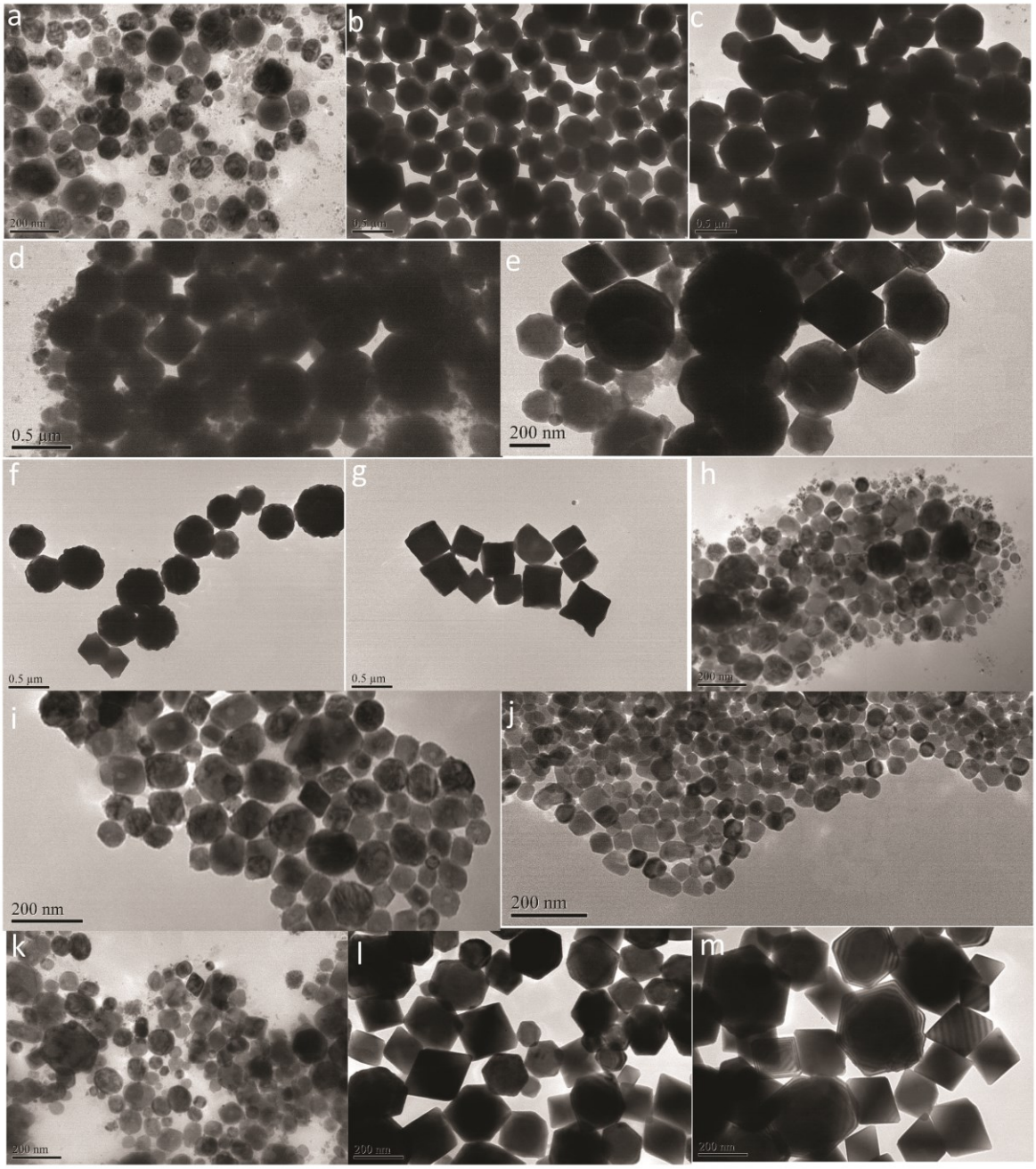

Figure1 TEM images of a S2, b S3, c S4 d S5, e S6, f S8, g S9, h S10, i S11, j S12, k S13, l S14, m S15.

is kept to be 10 mL. S12 is prepared with 10 mL OLA, without OA. The average sizes of the S8-S11 are 481 nm, 426 nm, 73 nm, and 83 nm, respectively. It can be observed that the sizes of the nanocrystals decrease as the OLA amount increases. The average size of S12 is 46 nm. Reaction time is another experimental parameter to control nanoparticle growth. Usually, a long reaction time leads to large nanoparticles and increased crystallinity.[27–29] Figure 1k-m shows the TEM images of S13-S15. The average sizes of the S13, S4, S14, and S15 are 76 nm, 525 nm, 200 nm, and 250 nm, corresponding to the reaction time of 1 h, 2 h, 4 h, and 6 h, respectively. The sizes increase from 76 nm to 525 nm as the reaction time increases from 1 h to 2 h. The sizes drop to 200 nm and 250 nm as the reaction time further increases to 4 h and 6 h. However, the crystallinity improves significantly as the reaction time increases to 4 h and 6 h, which is reflected from the sharp and smooth edges of the cubes in the TEM images (Fig. 1l and m).

Figure 2 shows the magnetic hysteresis loop of S3 and S12. Typical paramagnetic properties of MnO can be confirmed from the curves, which is consistent with the results of Yu.[30] The magnetization of S12 at the 40000 Oe is much higher than that of the S3. This is explained by the smaller size of S12 (46 nm) compared to S3 (387 nm). Smaller nanoparticles with more

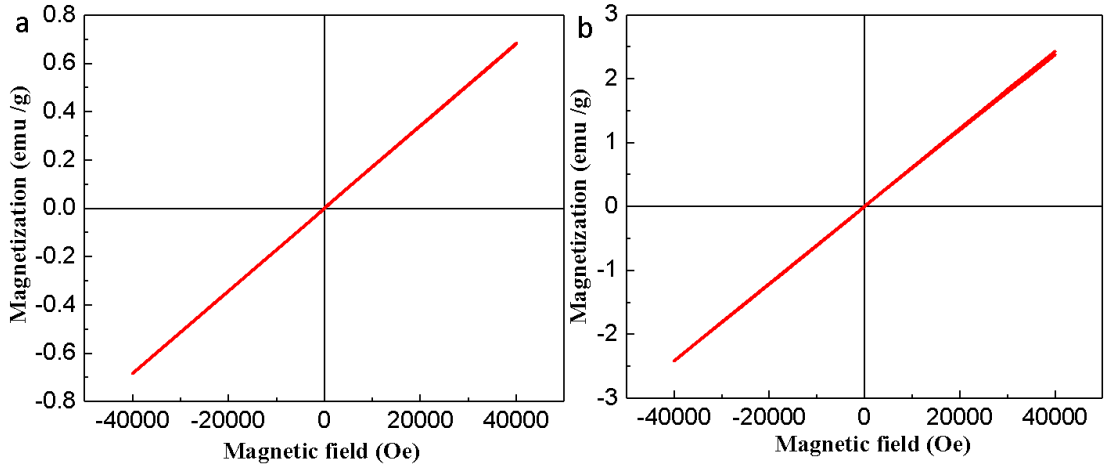

Figure 2 a and b show M-H loops of sample S3 and S12, respectively.

uncompensated surface spins exhibit higher magnetization according to the literature.[31] Therefore, our results are consistent with the literature results.

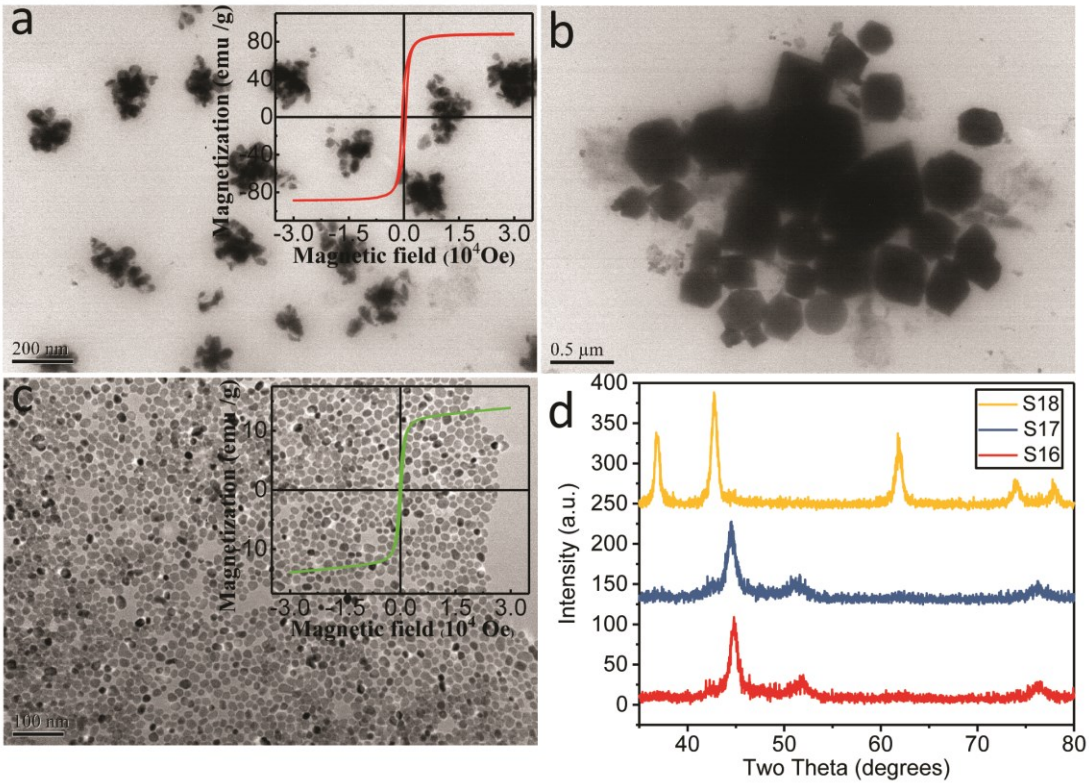

Figure 3 a TEM image of S16. b TEM image of S17. c TEM image of S18. The inset of figure a and c show the corresponding M-H loops. d XRD diffraction patterns of S16, S17, and S18.

The same experimental conditions are also used to prepare Co and CoO nanoparticles. Only three samples with pure phases can be obtained including S16-S18. Other samples prepared with similar experimental parameters with MnO reaction show the mixture phase of Co and CoO. Figure 3a shows the TEM image of S16 prepared with 10 mL OA and 20 mL OLA at 300 ºC. The size of S16 is ~50 nm. The inset of figure 3a is the M-H loops of S16. Typical magnetic properties are observed with a saturation magnetization of 88.2 emu/g, which is consistent with the literature results of metallic Co.[32] Figures 3b shows the TEM image of S17. It can be seen that the size of

S17 increases to ~500 nm compared to S16, which is explained by the amount of OLA. More OLA results in nanoparticle growth toward large sizes.[25,33–36] Figure 3 c shows the TEM image of S18. The average size of ~20 nm is obtained from the TEM image. The inset of figure 6c shows the M-H loop of S18. A coercivity of 250 Oe is obtained due to the uncompensated spins on the surface of the nanoparticles.[18] Figure 3d shows the XRD diffraction patterns of S16, S17, and S18. S16 and S17 can be indexed into hexagonal close-packed phases according to the standard card of JCPDS 45-1027. XRD result of S18 shows that cubic CoO nanocrystals (JCPDS card no. 48- 1719) are obtained. We believe Mn metal is not stable as Co, leading to Mn metal reacts with oxygen to produce MnO. However, in the case of Co. Co is stable in the reaction. Therefore, Co meatal can be obtained in a similar reaction.

Similar experimental procedures to MnO reaction are employed to prepare Ni-based nanoparticles. Only S19, S20, and S21 with pure phase Ni nanoparticles are obtained. Figures 4a,

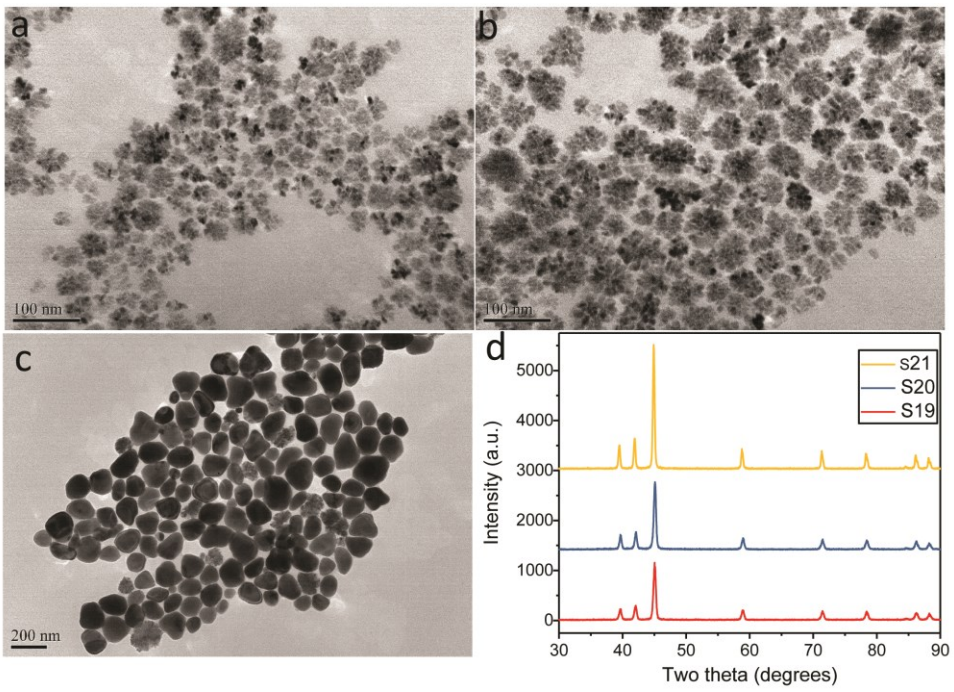

Figure 4 TEM image of a S19, b S20, and c S21. XRD diffraction patterns of d S19, e S20, f S21. The insets of figure 7a and c show the corresponding M-H loops.

b, and c show the TEM images S19-S21. The average sizes of S19, S20, and S21 are 80 nm, 80 nm, and 200 nm, respectively. S19 and S20 show that large nanoparticles are composed of smaller nanoparticles of ~10 nm. S19, S20, and S21 are indexed to cubic phase Ni nanoparticles (JCPDS: 45-1027) shown in figure 4d, e, f.

Co and CoO nanoparticles can be used for magnetic concentration cells.[37,38] Magnetic nanoparticles are attached with citric acid molecules and serve as carriers for the citric acid molecules.[37,38] Figure 5 shows the device performance of the concentration cells based on S16 and S18. It can be seen that the current and voltage values are 4 μA and 0.04 V, for the devices based on Co nanoparticles S16. However, the current and voltage values are 0.4 μA and 0.005 V,

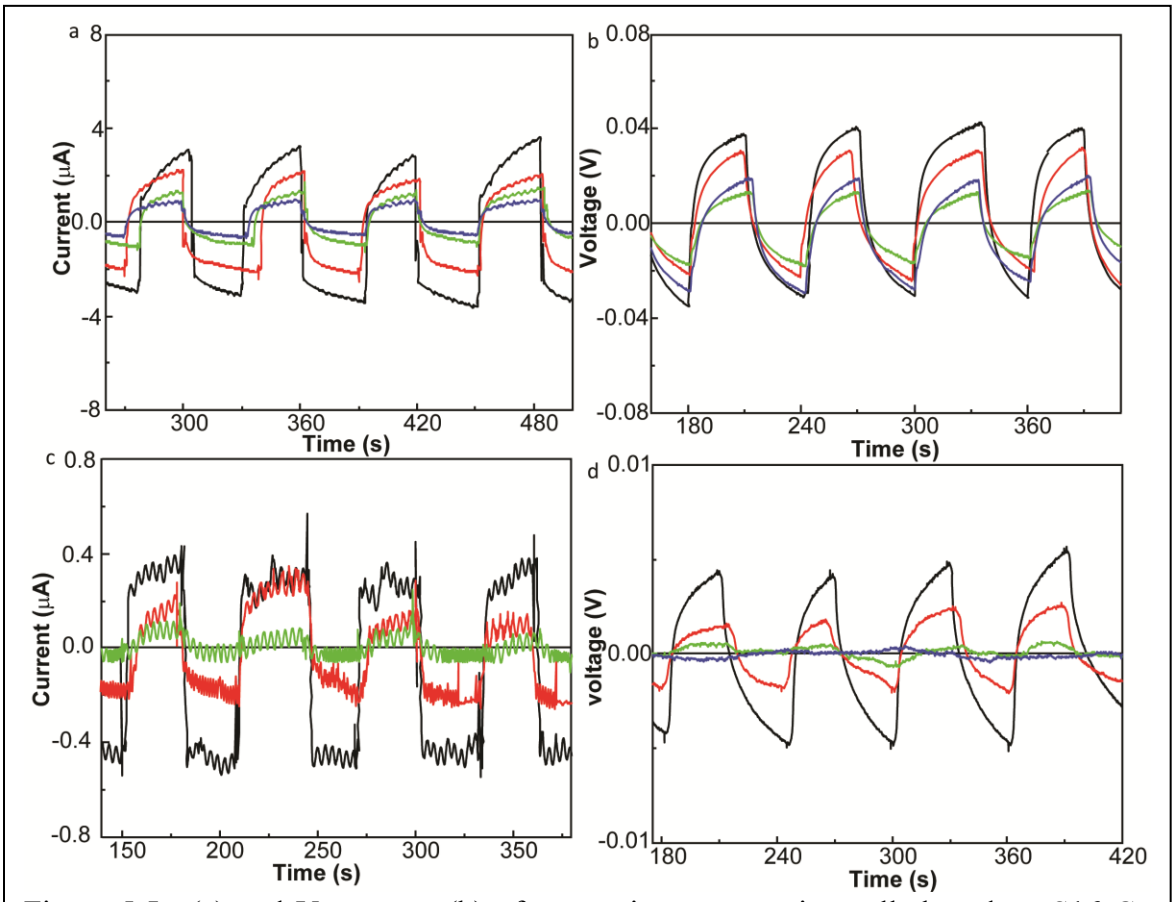

Figure 5 I-t (a) and V-t curves (b) of magnetic concentration cells based on S16 Co nanoparticles. I-t (c) and V-t (d) curves of magnetic concentration cells based on S18 CoO nanoparticles.

for the devices based on CoO nanoparticles S18. This is explained by the magnetic properties of the Co and CoO nanoparticles.[37,38] The Co nanoparticles show a high saturation magnetization than that of CoO. In addition, smaller particle sizes of Co nanoparticles are another reason for the high performance, leading to more citric acid molecules adsorbed on the particle surface.

Conclusion

MnO, Co, CoO, and Ni nanoparticles are synthesized by thermal decomposition of metal 2, 4-pentanedionates at different temperatures using OA, OLA, and ODE as ligands. MnO nanoparticles with different sizes (46-500 nm) are synthesized by the ligand ratios, reaction temperatures, and precursor concentrations. The prepared MnO nanoparticles show typical paramagnetic properties. Co nanoparticles with different sizes are also synthesized as the amount of OLA is larger than that of OA. CoO nanoparticles are obtained as only OLA are used as ligand, without OA. Ni nanoparticles in the size range of 80-200 nm are synthesized as similar experimental parameters are used in the reaction. Co and CoO nanoparticles are also studied by magnetic concentration cells. It shows that the cell performance of Co nanoparticles is much higher than that of CoO due to the high magnetization intensity and the smaller sizes.

Acknowledgment

This work is supported by NSF grant # 1912876. The CHI-604E Electrochemical workstation is supported by NSF grant #1332444. The XRD used in this work is supported by the U.S. Army Engineer Research and Development Center (W912HZ-16-2-0021). Work at UW was supported by the National Science Foundation under grant no. DMR-1710512 and DOE Office of Basic Energy Science (DE-SC0020074).

[1] I. Robinson, M. Volk, L.D. Tung, G. Caruntu, N. Kay, N.T. Thanh, Synthesis of Co Nanoparticles by Pulsed Laser Irradiation of Cobalt Carbonyl in Organic Solution, J. Phys. Chem. C. 113 (2009) 9497–9501. https://doi.org/10.1021/jp9014564.
[2] T. Toda, H. Igarashi, H. Uchida, M. Watanabe, Enhancement of the Electroreduction of Oxygen on Pt Alloys with Fe, Ni, and Co, J. Electrochem. Soc. 146 (1999) 3750. https://doi.org/10.1149/1.1392544.
[3] H. Sun, S.Y. Lee, C.S. Lee, Physical Chemistry Research Articles Published in the Bulletin of the Korean Chemical Society: 2003-2007, (n.d.) 13.
[4] A. Jordan, R. Scholz, P. Wust, H. Fähling, R. Felix, Magnetic fluid hyperthermia (MFH): Cancer treatment with AC magnetic field induced excitation of biocompatible superparamagnetic nanoparticles, J. Magn. Magn. Mater. 201 (1999) 413–419. https://doi.org/10.1016/S0304-8853(99)00088-8.
[5] P. Tartaj, M. a del P. Morales, S. Veintemillas-Verdaguer, T.G. lez-Carre o, C.J. Serna, The preparation of magnetic nanoparticles for applications in biomedicine, J. Phys. Appl. Phys. 36 (2003) R182–R197. https://doi.org/10.1088/0022-3727/36/13/202.
[6] M. Hoehn, E. Küstermann, J. Blunk, D. Wiedermann, T. Trapp, S. Wecker, M. Föcking, H. Arnold, J. Hescheler, B.K. Fleischmann, W. Schwindt, C. Bührle, Monitoring of implanted stem cell migration in vivo: A highly resolved in vivo magnetic resonance imaging investigation of experimental stroke in rat, Proc. Natl. Acad. Sci. 99 (2002) 16267–16272. https://doi.org/10.1073/pnas.242435499.
[7] M. Todorovic, S. Schultz, J. Wong, A. Scherer, Writing and reading of single magnetic domain per bit perpendicular patterned media, Appl. Phys. Lett. 74 (1999) 2516–2518. https://doi.org/10.1063/1.123885.
[8] Synthesis and Characterization of CoO, Co3O4, and Mixed Co/CoO Nanoparticules | Chemistry of Materials, (n.d.). https://pubs.acs.org/doi/abs/10.1021/cm991003h (accessed March 6, 2021).
[9] Y. Ye, F. Yuan, S. Li, Synthesis of CoO nanoparticles by esterification reaction under solvothermal conditions, Mater. Lett. 60 (2006) 3175–3178. https://doi.org/10.1016/j.matlet.2006.02.062.
[10] X. Sun, Y.-W. Zhang, R. Si, C.-H. Yan, Metal (Mn, Co, and Cu) Oxide Nanocrystals from Simple Formate Precursors, Small. 1 (2005) 1081–1086. https://doi.org/10.1002/smll.200500119.
[11] download.pdf, (n.d.). http://citeseerx.ist.psu.edu/viewdoc/download?doi=10.1.1.83.9060&rep=rep1&type=pdf (accessed March 6, 2021).
[12] L.T. Lu, L.D. Tung, I. Robinson, D. Ung, B. Tan, J. Long, A.I. Cooper, D.G. Fernig, N.T.K. Thanh, Size and shape control for water-soluble magnetic cobalt nanoparticles using polymer ligands, J. Mater. Chem. 18 (2008) 2453–2458. https://doi.org/10.1039/B801800F.
[13] J. Jiao, S. Seraphin, X. Wang, J.C. Withers, Preparation and properties of ferromagnetic carbon-coated Fe, Co, and Ni nanoparticles, J. Appl. Phys. 80 (1996) 103–108. https://doi.org/10.1063/1.362765.
[14] D. Li, S. Komarneni, Microwave-Assisted Polyol Process for Synthesis of Ni Nanoparticles, J. Am. Ceram. Soc. 89 (2006) 1510–1517. https://doi.org/10.1111/j.1551-2916.2006.00925.x.

[15] V. Tzitzios, G. Basina, M. Gjoka, V. Alexandrakis, V. Georgakilas, D. Niarchos, N. Boukos, D. Petridis, Chemical synthesis and characterization of hcp Ni nanoparticles, Nanotechnology. 17 (2006) 3750–3755. https://doi.org/10.1088/0957-4484/17/15/023.
[16] Y.T. Jeon, J.Y. Moon, G.H. Lee, J. Park, Y. Chang, Comparison of the Magnetic Properties of Metastable Hexagonal Close-Packed Ni Nanoparticles with Those of the Stable Face-Centered Cubic Ni Nanoparticles, J. Phys. Chem. B. 110 (2006) 1187–1191. https://doi.org/10.1021/jp054608b.
[17] S. Chandra, A. Kumar, P.K. Tomar, Synthesis of Ni nanoparticles and their characterizations, J. Saudi Chem. Soc. 18 (2014) 437–442. https://doi.org/10.1016/j.jscs.2011.09.008.
[18] Q. Dai, J. Tang, The optical and magnetic properties of CoO and Co nanocrystals prepared by a facile technique, Nanoscale. 5 (2013) 7512–7519. https://doi.org/10.1039/C3NR01971C.
[19] Q. Dai, J. Tang, Magnetic properties of CoO nanocrystals prepared with a controlled reaction atmosphere, RSC Adv. 3 (2013) 9228–9233. https://doi.org/10.1039/C3RA40834E.
[20] G. Madras, B.J. McCoy, Temperature effects on the transition from nucleation and growth to Ostwald ripening, Chem. Eng. Sci. 59 (2004) 2753–2765. https://doi.org/10.1016/j.ces.2004.03.022.
[21] G. Madras, B.J. McCoy, Temperature effects during Ostwald ripening, J. Chem. Phys. 119 (2003) 1683–1693. https://doi.org/10.1063/1.1578617.
[22] X. Xue, R.L. Penn, E.R. Leite, F. Huang, Z. Lin, Crystal growth by oriented attachment: kinetic models and control factors, CrystEngComm. 16 (2014) 1419–1429. https://doi.org/10.1039/C3CE42129E.
[23] H.S. Dehsari, A.H. Ribeiro, B. Ersöz, W. Tremel, G. Jakob, K. Asadi, Effect of precursor concentration on size evolution of iron oxide nanoparticles, CrystEngComm. 19 (2017) 6694–6702. https://doi.org/10.1039/C7CE01406F.
[24] R.A. Harris, P.M. Shumbula, H. van der Walt, Analysis of the Interaction of Surfactants Oleic Acid and Oleylamine with Iron Oxide Nanoparticles through Molecular Mechanics Modeling, Langmuir. 31 (2015) 3934–3943. https://doi.org/10.1021/acs.langmuir.5b00671.
[25] A.B. Panda, G. Glaspell, M.S. El-Shall, Microwave Synthesis and Optical Properties of Uniform Nanorods and Nanoplates of Rare Earth Oxides, J. Phys. Chem. C. 111 (2007) 1861–1864. https://doi.org/10.1021/jp0670283.
[26] M.B. Mohamed, K.M. AbouZeid, V. Abdelsayed, A.A. Aljarash, M.S. El-Shall, Growth mechanism of anisotropic gold nanocrystals via microwave synthesis: formation of dioleamide by gold nanocatalysis, ACS Nano. 4 (2010) 2766–2772. https://doi.org/10.1021/nn9016179.
[27] A.-A. Litwinowicz, S. Takami, S. Asahina, X. Hao, A. Yoko, G. Seong, T. Tomai, T. Adschiri, Formation dynamics of mesocrystals composed of organically modified CeO2 nanoparticles: analogy to a particle formation model, CrystEngComm. 21 (2019) 3836–3843. https://doi.org/10.1039/C9CE00473D.
[28] Z.A. Zulkifli, K.A. Razak, W.N.W.A. Rahman, Effect of hydrothermal reaction time on size of bismuth oxide nanoparticles synthesized via hydrothermal method, AIP Conf. Proc. 1901 (2017) 020011. https://doi.org/10.1063/1.5010448.
[29] C. Duan, Y. Meng, Y. Wang, Z. Zhang, Y. Ge, X. Li, Y. Guo, D. Xiao, High-crystallinity and high-rate Prussian Blue analogues synthesized at the oil–water interface, Inorg. Chem. Front. 8 (2021) 2008–2016. https://doi.org/10.1039/D0QI01361G.

[30] Folic Acid-Conjugated MnO Nanoparticles as a T1 Contrast Agent for Magnetic Resonance Imaging of Tiny Brain Gliomas | ACS Applied Materials & Interfaces, (n.d.). https://pubs.acs.org/doi/10.1021/am505223t (accessed March 4, 2021).
[31] C.-C. Lin, C.-J. Chen, R.-K. Chiang, Facile synthesis of monodisperse MnO nanoparticles from bulk MnO, J. Cryst. Growth. 338 (2012) 152–156. https://doi.org/10.1016/j.jcrysgro.2011.10.022.
[32] X. Sun, A. Gutierrez, M.J. Yacaman, X. Dong, S. Jin, Investigations on magnetic properties and structure for carbon encapsulated nanoparticles of Fe, Co, Ni, Mater. Sci. Eng. A. 286 (2000) 157–160. https://doi.org/10.1016/S0921-5093(00)00628-6.
[33] X. Lu, H.-Y. Tuan, B.A. Korgel, Y. Xia, Facile Synthesis of Gold Nanoparticles with Narrow Size Distribution by Using AuCl or AuBr as the Precursor, Chem. Weinh. Bergstr. Ger. 14 (2008) 1584–1591. https://doi.org/10.1002/chem.200701570.
[34] L.J. Treadwell, T.J. Boyle, N.S. Bell, Mark.A. Rodriguez, B.R. Muntifering, K. Hattar, Impact of oleylamine: oleic acid ratio on the morphology of yttria nanomaterials, J. Mater. Sci. 52 (2017) 8268–8279. https://doi.org/10.1007/s10853-017-1042-5.
[35] M.A.B. Aissa, B. Tremblay, A. Andrieux-Ledier, E. Maisonhaute, N. Raouafi, A. Courty, Copper nanoparticles of well-controlled size and shape: a new advance in synthesis and self-organization, Nanoscale. 7 (2015) 3189–3195. https://doi.org/10.1039/C4NR06893A.
[36] F. Lan, J. Bai, H. Wang, The preparation of oleylamine modified micro-size sphere silver particles and its application in crystalline silicon solar cells, RSC Adv. 8 (2018) 16866–16872. https://doi.org/10.1039/C8RA02620C.
[37] Q. Dai, K. Patel, G. Donatelli, S. Ren, Magnetic Cobalt Ferrite Nanocrystals For an Energy Storage Concentration Cell, Angew. Chem. Int. Ed Engl. 55 (2016) 10439–10443. https://doi.org/10.1002/anie.201604790.
[38] Y. Zhang, G. Rimal, J. Tang, Q. Dai, Synthesis of NiFe2O4 nanoparticles for energy and environment applications, Mater. Res. Express. 5 (2018) 025023. https://doi.org/10.1088/2053-1591/aaacde.